Large halocline variations in the Northern Baltic Proper and associated meso- and basin-scale processes*

OCEANOLOGIA, 48 (S), 2006.
pp. 91–117.

KEYWORDS
Baltic Sea
Gulf of Finland
Halocline
Currents
Mesoscale eddies

Jüri Elken[1]
Pentti Mälkki[2]
Pekka Alenius[2]
Tapani Stipa[2]

[1] Marine Systems Institute,
Tallinn University of Technology,
Akadeemia tee 21, EE–12618 Tallinn, Estonia;

e-mail: elken@phys.sea.ee

[2] Finnish Institute of Marine Research,
Dynamicum, Erik Palménin aukio 1,
PO Box 2, FIN–00561 Helsinki, Finland

Received 5 December 2005, revised 12 May 2006, accepted 15 May 2006.

Abstract

The Northern Baltic Proper is a splitting area of the Baltic Sea saline water route towards the two terminal basins – the Gulf of Finland and the Western Gotland Basin. Large halocline variations (vertical isopycnal displacements of more than 20 m, intra-halocline current speeds above 20 cm s^{-1}) appear during and following SW wind events, which rapidly increase the water storage in the Gulf of Finland and reverse the standard estuarine transport, causing an outflow in the lower layers. In the channel of variable topography, basin-scale barotropic flow pulses are converted into baroclinic mesoscale motions such as jet currents, sub-surface eddies and low-frequency waves. The associated dynamics is analysed by the results from a special mesoscale experiment, routine observations and numerical modelling.

* This study has been partly supported by grants Nos 2194 and 5868 from the Estonian Science Foundation.

1. Introduction

Temporal variability in the physical regime of large dilution basins such as the Baltic Sea, Gulf of St. Lawrence, Hudson Bay and many others is caused primarily by interannual and decadal variations in seasonal freshwater and ocean water inflow pulses, wind stress events and air–sea heat fluxes (Matthäus & Frank 1992, Saucier & Dionne 1998, Gustafsson & Andersson 2001, Tian et al. 2001, Winsor et al. 2001). An important aspect of diluted seas is the deep saline layer, separated from the surface layers by a halocline. The dynamics of the halocline is to a great extent controlled by the deep topographic basins and channels. As the basin dimensions are much larger than the baroclinic Rossby deformation radius, the internal basin dynamics is rather complex and is influenced by mesoscale processes (eddies, meandering jet currents, fronts etc.) that develop above variable topography. Narrower deepwater passages are often characterised by the average channel flow/overflow regime (Stigebrandt & Gustafsson 2003), which is modified by the barotropic flows due to sea-level gradients (Lehmann & Hinrichsen 2002) and mesoscale processes (Zhurbas et al. 2004). The hydrographic and ecological regimes of the diluted seas are essentially influenced by the advection and mixing processes occurring in the halocline and in the deepwater.

In the Baltic Sea, a tideless estuarine system, a large number of investigations of saline water inflows and related halocline dynamics have been conducted in recent years in the western part of the sea (Omstedt et al. 2004, Piechura & Beszczyńska-Möller 2004). These studies have been motivated by the need to understand and quantify the processes behind the alternation of deepwater stagnation periods and renewal events. This is important for the functioning of the marine system and the regional climate (Stigebrandt & Gustafsson 2003, Omstedt et al. 2004).

Recent investigations of diapycnal mixing in the Gotland Basin, the largest and central deep basin of the Baltic Sea, have shown that the vertical fluxes are too small to close the Baltic water cycle in this basin (Stigebrandt et al. 2002, Lass et al. 2003). Model calculations, done with either a simple budget model (Kõuts & Omstedt 1993) or an advanced 3-dimensional (3D) circulation model (Meier & Kauker 2003), have also shown that the mean deepwater import to the Gotland Basin is roughly equal to the export towards the Northern Baltic Proper, a basin that further splits towards two deepwater terminal areas – the Gulf of Finland and the Western Gotland Basin. If the average deepwater flow into the Northern Baltic Proper is taken to be 20 mSv (20 000 m^3 s^{-1}), the flow continuity yields a vertical speed of the halocline rise of 16 m per year in the Northern Baltic Proper and its extensions. On a yearly scale, this rise has to be

compensated for by halocline erosion, resulting in large seasonal variations of temperature, salinity and density (Matthäus 1984). Indeed, Dietrich (1948) already noted that at monitoring station BMP H2 (Fig. 1), the seasonal variation in salinity amounted to 1 PSU at depths of 80 to 150 m, which is higher than at other Baltic monitoring stations.

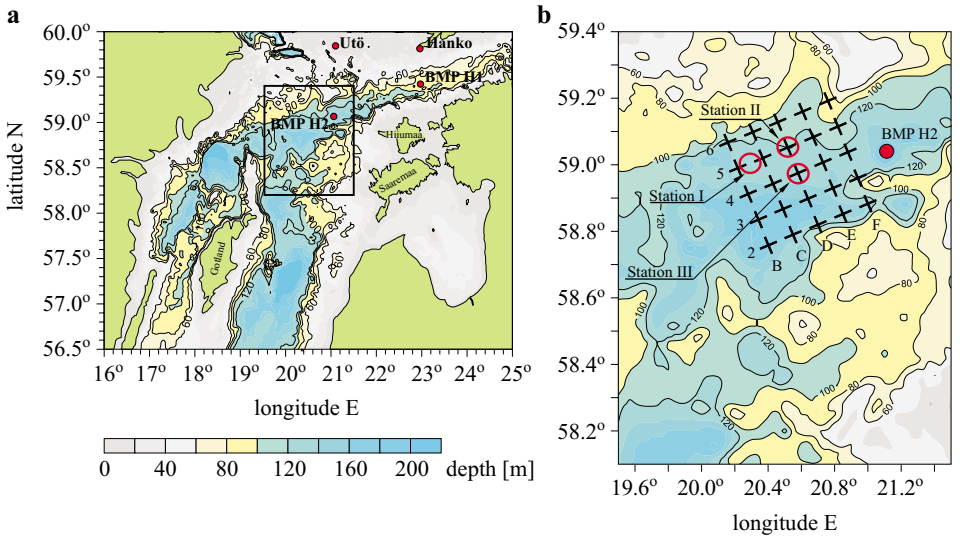

Fig. 1. Maps of the Northern Baltic Proper (a) with routine observation stations, shown by red dots, and the study area of the mesoscale dynamics experiment of 1982 (b; on the left map in the box). On the map of the study area, the crosses denote the CTD sampling locations and the red circles denote the mooring station locations. On both maps, the axes describe the decimal geographical coordinates N, E

The aim of the present study is is to provide an insight into the mesoscale and basin-scale processes in the Northern Baltic Proper. We are interested, in particular, in learning whether lateral advection processes contribute significantly to the large halocline variations noted above. An understanding of this is important in the context of further studies of Baltic Sea water and nutrient cycles under changing climatic conditions.

On inspecting the observational material available on the Northern Baltic Proper, we found that the most complete and valuable data set comes from the mesoscale dynamics experiment conducted in 1982. This experiment, with its hitherto unpublished results, is the focus of the present paper. Following the description of individual observations, a concept

governing meso- and basin-scale processes will be formulated. This concept is further checked against the data of routine observations and numerical modelling, and conclusions will be drawn from the discussion on the process mechanisms and their impact.

2. Material and methods

2.1. The 1982 experiment on mesoscale dynamics

The study area was located in the middle of the Northern Baltic Proper, as shown in Fig. 1. At the level of 100 m the connection from the Gotland Basin, lying to the south, is 11 km wide in the main passage and 6 km in the smaller, eastern passage. To the east of the main passage, the area extends 50 to 80 km in a north–south direction, which is far more than the baroclinic Rossby radius, which remains within the range of 6–10 km (Fennel et al. 1991, Alenius et al. 2003). The maximum depth amounts to 188 m. To the east, the area extends as a deep, contracting channel towards the Gulf of Finland. Over a distance of 110 km of the channel length, the channel width decreases to about 10 km north of Hiiumaa. To the west, the area extends towards the Landsort Deep, with the narrowest passage being 25 km wide and 130 m deep.

The investigations were carried out on the r/v 'Ayu-Dag' (Department of the Baltic Sea, Tallinn) and 'Aranda' (Finnish Institute of Marine Research, Helsinki) in the last days of August and in September 1982. The core of the experiment was a series of repeated CTD sampling surveys conducted in a 5 × 5 stations grid with a 5 nm (nautical miles) grid step. The x-axis of the grid was parallel to the centre line of the Gulf of Finland and to the local large-scale bottom topography. The y-axis was directed towards 338°, that is 22° counterclockwise from north. The corner stations of the CTD sampling grid in 'chess' notation were B2 (58°45.6′N, 20°24.3′E), B6 (59°04.0′N, 20°10.0′E), F2 (58°53.0′N, 21°00.0′E) and F6 (59°11.5′N, 20°45.6′E).

In total, six surveys of the grid were made (Table 1). The three mooring stations were located inside the grid, forming a triangle that had its shorter sides along the axes of the grid (Table 2). Current meters were installed at depths of 15, 30 and 90 m at all the three stations. Thermistor chains were installed at stations I and II, covering a layer from about 15 to 40 m. The mooring stations recorded with a sampling interval of 5 min from 31 August to 23 September 1982, with the exception of currents at 30-m depth at station II, where successful recording took place until 11 September.

Table 1. CTD surveys of the grid given in Fig. 1

Survey number	Survey period	Ship
1	29–30 August 1982	'Ayu-Dag'
2	02–03 September 1982	'Aranda'
3	03–04 September 1982	'Aranda'
4	06–07 September 1982	'Aranda'
5	10–11 September 1982	'Ayu-Dag'
6	20–21 September 1982	'Ayu-Dag'

Table 2. Location of mooring stations with 'Aanderaa' current meters and thermistor chains

Station	Latitude	Longitude	Grid location	Station depth [m]
station I	59 00.4′N	20 17.4′E	between B5 and C5	154
station II	59 03.3′N	20 31.3′E	D5	127
station III	58 58.9′N	20 34.8′E	D4	136

The data were processed using standard methods (e.g. ICES 1989). The CTD probes on both ships were calibrated accurately and no bias was detected in the data. In analysing the non-synchronous CTD data, special attention was paid to the aliasing problem. In the optimal interpolation procedure for drawing the synoptic maps, noise-to-signal ratio estimates of 0.1–0.2 were introduced to suppress high-frequency noise (e.g. Aitsam & Elken 1982). The main mesoscale features were resolved on the 5-nm grid, because within and below the halocline the horizontal correlation scales (the distance where the correlation drops below 0.2) were 11–13 nm for isopycnal displacements and dynamic topography, and 6–7 nm for layer thickness between isopycnals. Isopycnals were defined as surfaces of constant potential density, referenced to the surface.

2.2. Routine observational data involved

Reliable meteorological observations nearest the Northern Deep were made by the Finnish Meteorological Institute on Utö Island (Fig. 1a). Their data were used to study the wind forcing events in this particular sea area.

The sea level data used in this study were taken from the Finnish stations Hanko (Fig. 1a), Helsinki and Hamina (not shown), operated by the Finnish Institute of Marine Research. In the analysis, the object of primary interest was rapid water storage variation in the Gulf of Finland, which occurs as a result of accumulative wind effects and the related baroclinic response in the deep layers.

Hydrographic variations in the water column were studied over a longer period (1979–98) on the basis of the HELCOM COMBINE monitoring data made available through the marine environment assessment procedure (HELCOM 2002). The main monitoring stations of interest are BMP H2 (59°03′N, 21°07′E) and BMP H1 (59°28′N, 22°53′E), shown in Fig. 1a. For estimating the hydrographic differences between the stations, the original temperature and salinity data were gridded into monthly vertical profiles using optimal interpolation (with the estimated noise-to-signal ratio and correlation scales) as described by Elken (ed.) (1996). Near both these stations, episodic high-resolution data from special studies were also included.

2.3. Model data involved

The observational material was complemented by the results obtained from a 3D numerical model of the Baltic Sea, the FIMR operational model BalEco (Stipa et al. 2003), which has a 6 nm resolution and 21 vertical layers. The model is based on the MITgcm (Marshall et al. 1997), which has undergone rigorous validation in a large number of process studies.

The model was initialised with fields from the HELCOM COMBINE monitoring performed by FIMR in January–February 2004. Subsequently, the initial state was integrated forward in time, with the model using atmospheric boundary conditions from the ECMWF forecast results, as well as with lateral boundary conditions imposed by the main rivers of the Baltic.

Later HELCOM COMBINE results from early June and early August 2004 were assimilated into the model with a simple nudging scheme. A validation of the operational model results against the independent Alg@line data set was presented by Kiiltomäki & Stipa (2006) and Kiiltomäki et al. (2005).

3. Results

3.1. The mesoscale dynamics in 1982

3.1.1. Wind forcing and water level

During the second half of August, a number of depressions passed over Finland, bringing predominantly moderate SW winds to the Northern Baltic Sea. During the first days of September, a large depression proceeded eastwards over the Northern Baltic, bringing stronger W winds, which by 5 September veered NW and then abated for the next two days. This was followed by a fast-moving area of low pressure that brought strong W winds to the Northern Baltic. Starting on 9 September, a large high-pressure

field covered the entire Baltic, moving slowly towards the east. A period of variable winds followed, with predominantly, but not persistently SW winds.

Fig. 2 shows the wind vectors at the nearest meteorological station of Utö. Before and during the experiment, moderate winds predominantly from the SW, W or NW at speeds from 7 to 10 m s^{-1} were observed. SE winds prevailed from 17 to 19 August, and on 27 and 31 August; S winds on 21 August and on 1, 8, 11 and 21 September. Two episodes of strong winds from the NNW also occurred, one on 9 September, the other on 14 September. Winds of variable direction were recorded from 23 to 26 August. During the moored measurements, from 31 August to 23 September, the average wind speed was 6.3 m s^{-1}. The resultant wind speed was 5.9 m s^{-1} from the WSW (243°) direction.

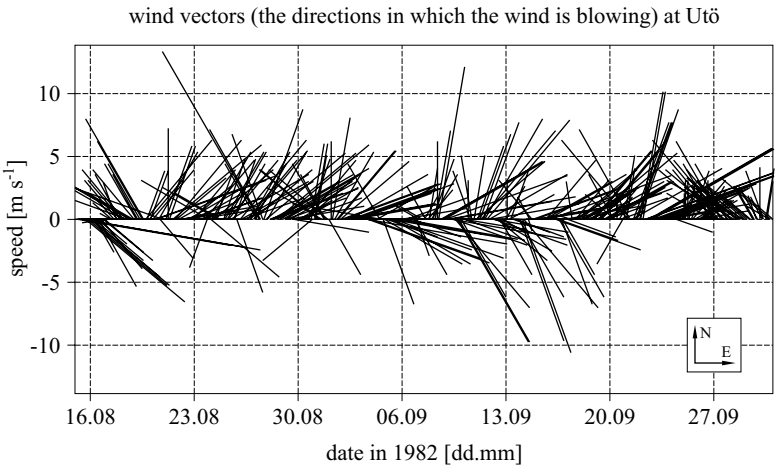

Fig. 2. Wind vectors observed at Utö meteorological station

Water-level oscillations off the northern coast of the Gulf of Finland showed low frequency changes in August–September 1982 (Fig. 3). Before the experiment, during the last week of August, the water level was about 20 cm above the mean sea level. The sea level dropped some 10–20 cm during the last days of August and then rose 30–50 cm in 3–4 days. This fall in the water level was due to the dominant SW wind backing SE. The rapid water-level increase was related to the re-establishment of the SW winds. The amplitudes of this sea-level were highest at the easternmost Hamina station. The phase of the sea-level rise propagated on the northern coast of the Gulf of Finland cyclonically from east to west. After 4 September, the sea level gradually fell some 20 cm during the moored observation period until 23 September.

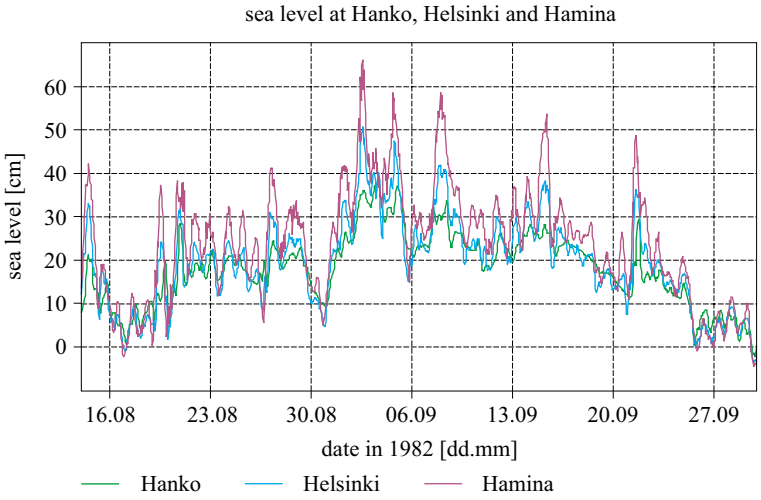

Fig. 3. Sea levels observed at the coastal stations of Hanko (see Fig. 1), Helsinki (about 130 km east of Hanko) and Hamina (about 150 km east of Helsinki)

3.1.2. Repeated CTD surveys

The temperature, salinity and density stratification (Fig. 4) showed a clear three-layer structure, as is common in the area in summer (Haapala & Alenius 1994). During the whole experiment the upper layer of the sea, from the surface to 20–25 m depth, was vertically homogeneous. The main

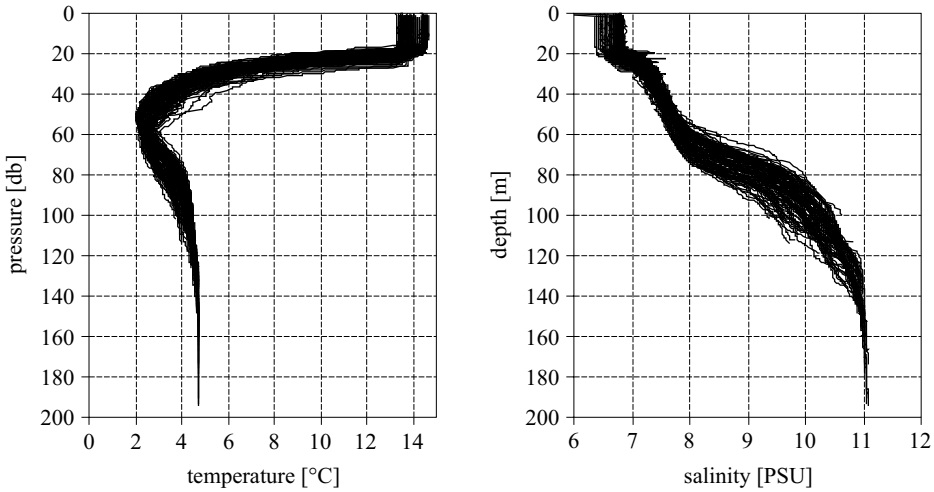

Fig. 4. Cluster temperature (left) and salinity (right) profiles measured from 2 to 7 September on board r/v 'Aranda' (surveys 2–4 in Table 1, 3 × 25 stations with a spacing of 5 miles)

thermocline was also a jump layer for an increase in salinity with depth. In the mid-depths between the thermocline and halocline, there was a layer of cold water. The main halocline began from 60–80 m depth. The highest variability in salinity occurred in the halocline from 60 m down to 110 m.

The motion of surface water masses was evident from the observed patterns of salinity. Results from the 1st survey revealed the propagation of more saline waters of the Baltic Proper to the north on the eastern side of the grid, contrary to the usual bi-directional flow scheme, where in the north less saline waters appear, flowing out of the Gulf of Finland. Twelve days later the invading Baltic Proper waters increased the upper layer salinity by 0.2–0.3 PSU, with a maximum value of 7.1 PSU, as observed in the 5th survey. This advection from the south was also evident in the temperature data. After the change in the SW winds, by the time of the 6th survey, smaller amounts of saline waters of the Gulf of Finland of < 6.8 PSU had again penetrated into the study area.

Variations in the mass field were studied by the analysis of isopycnal depths (surfaces of constant potential density anomaly σ) and dynamic

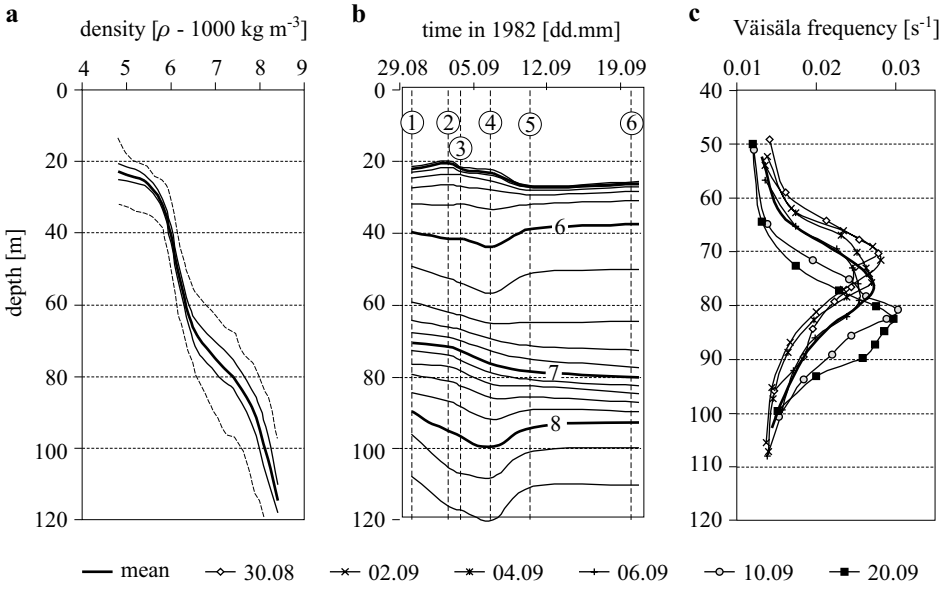

Fig. 5. Mean density stratification during 6 surveys based on isopycnal depth analysis plotted against the mean isopycnal depths: mean (bold line), 25% and 75% quartiles (thin lines), minimum and maximum (dashed lines) of isopycnal depths of the whole data set of 6 surveys (a), temporal change in mean isopycnal depths of the 6 individual surveys, survey times shown with numbered labels (b), and Väisälä frequency based on the mean isopycnal depths of the 6 individual surveys and the overall mean (c)

topography. The variability in isopycnal depths (Fig. 5a) increased from $\sigma = 6.0$ kg m^{-3} (mean depth 40 m) downwards, together with a reduction in the density gradient in the deep layers. At the deep level $\sigma = 8.2$ kg m^{-3} (mean depth 103 m) the maximum difference between isopycnal depths reached 36 m and the difference of 75% and 25% quartiles amounted to 12 m. With the average area depth around 140 m, the 'amplitude' to depth ratio was predominantly around 0.04, but reached a maximum value of 0.13.

Within the overall mass field variations, the temporal change in the mean stratification of the 6 individual surveys was quite significant, as shown in Fig. 5b,c. The maximum Väisälä frequency $N_{\max}$ was observed at isopycnals 7.0–7.2 kg m^{-3}. As time passed, the depth of $N_{\max}$ dropped rapidly in 8 days from 70 m (2nd survey) to 80 m (5th survey). Below the $N_{\max}$ layer, isopycnals 7.8–8.4 kg m^{-3} deepened from the 1st survey to the 4th survey in 8 days by 8–12 m (at a rate of 1–1.5 m day^{-1}) but later reverted to the levels of the 1st survey. Based on the evidence of small diapycnal fluxes in the halocline (Lass et al. 2003), the stratification behaviour depicted in Fig. 5b could be explained by the intrusion of deepwater of intermediate density below $N_{\max}$ levels and its further export from the area. Note that this deepwater event was coherent with the rapid increase in the water level observed in the Gulf of Finland (Fig. 3).

The within-survey mass field variability was further studied by analysing isopycnal displacements $\xi_k(n,i) = z_k(n,i) - \overline{z_k}(n)$ of the density level σ_k from the mean isopycnal depth $\overline{z_k}(n) = {}^i\overline{z_k(n,i)}$, where n is the survey index, i is the profile index within the survey, and the index before the bar denotes the set of averaging. The set of survey-mean isopycnal depths resembles the reference state of the minimum potential energy in the area, assuming adiabatic levelling of actual isopycnal surfaces. Available potential energy APE per unit mass, arising from the meso- and small-scale motions of small amplitudes, is defined in the Boussinesq approximation as

$$APE_k(n) = \frac{1}{2}\overline{N_k}(n)^2\, {}^i\overline{\xi_k(n,i)^2}, \tag{1}$$

where $\overline{N_k}(n)^2 = {}^i\overline{N_k(n,i)^2}$ is the survey-mean squared Väisälä frequency. Although expression (1) is not suitable for studying the energetics of basin-wide circulation (Huang 1998), it is an energetic measure of isopycnal displacements in a limited area. Note that the mean APE over a layer from $\overline{z_{k1}}(n)$ to $\overline{z_{k2}}(n)$ is fully proportional to the mean isopycnal depth variance over isopycnals from σ_{k1} to σ_{k2}.

Isopycnal displacements can be decomposed into vertical modes by empirical orthogonal functions (EOF) $f_m(k)$ as

$$\xi_k(n,i) = \sum_{n=1}^{M} a_m(n,i) f_m(k), \tag{2}$$

where the number of modes M equals the number of isopycnal levels involved in the analysis and $f_m(k)$ are calculated as eigenvectors of the covariance matrix

$$^{n,i}\overline{\xi_p(n,i)\xi_q(n,i)}.$$

The APE was concentrated in the halocline below 60 m as shown in Fig. 6a. The observed levels were highest around 80 m depth, reaching 100 cm^2 s^{-2}. The vertical structure of isopycnal displacements below 60 m was dominated by the 3 first modes (Fig. 6b), which covered 62%, 25% and 5% of the total variance, respectively. The level of zero displacement of the second EOF was at a depth around 85 m.

During the observation period the intensity of the mesoscale mass field variability increased considerably. Following the wind pulses and rapid water level rise (Fig. 3), the APE and isopycnal displacement variance increased 3-fold in 8 days from the 1st to the 4th survey (Fig. 6c). The halocline mean APE levels obtained – from 60 to 80 cm^2 s^{-2} – were quite high compared to the eddy energetics observed in the Gotland Deep. Of the 21 mesoscale surveys conducted historically in the Gotland Deep area, only 4 revealed a mean APE above 40 cm^2 s^{-2} in the energy-containing layer of 60–150 m (Elken (ed.) 1996). According to the vertical mode structure, the contribution of the 2nd mode was comparable to that of the 1st mode at the initial stage of isopycnal variance growth until the 3rd survey, but later the 1st mode clearly dominated.

The evolution patterns of the halocline $N_{\max}$ layer are shown in Fig. 7 by the depths of the 7.0 kg m^{-3} potential density layer.

From a quite flat halocline surface during the 1st survey, with a slight doming in the centre of the area, immersion of the halocline had started by the 2nd survey in the eastern and north–eastern parts of the area and had extended by the 4th, 5th and 6th surveys considerably both in coverage and intensity. Already in the 4th survey the halocline was strongly tilted (about 1 m to 1 km), with a drop in its depth from about 70 m in the southwest corner to 83–85 m in the north–eastern part. This tilted pattern of the halocline, although disturbed by meanders and isolated high/low features, remained until the end of the experiment. The eddy-like doming observed at station D4 during the 2nd and 3rd surveys is discussed in some detail in the following analysis.

Fig. 8 represents the dynamic topography of the 30-dbar level relative to the 90-dbar level, together with low-passed relative current vectors between the corresponding depth levels. The integration limits of the specific volume

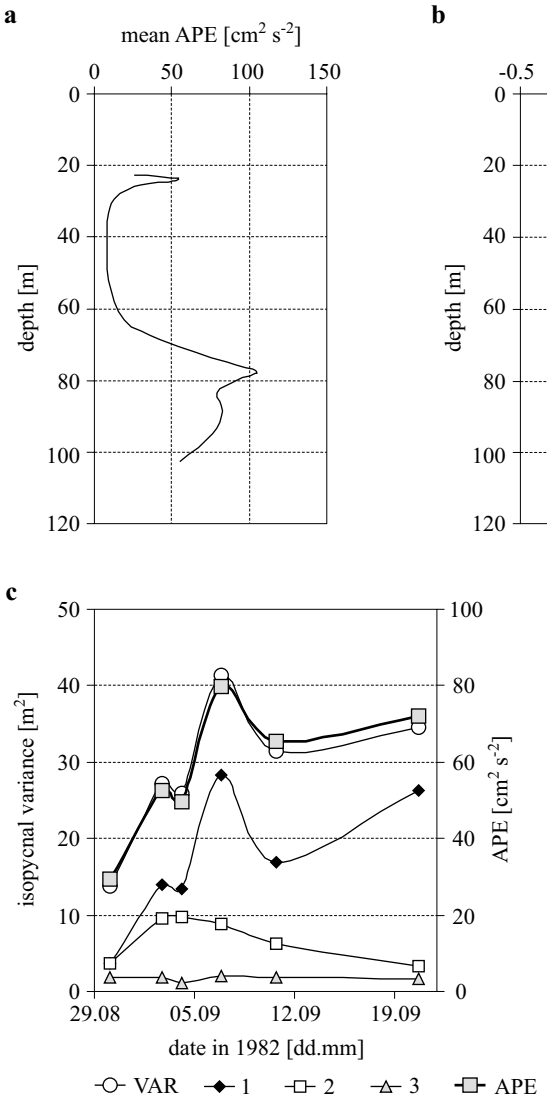

Fig. 6. Mean (over all surveys) vertical profiles of available potential energy density per unit mass (a) and 3 first normalised EOF of isopycnal displacements in the range $\sigma = 6.4 - 8.2$ kg m^{-3} (b) plotted against the mean isopycnal depths, and temporal change in depth-mean (60–110 m) available potential energy, total variance and particular variance of 3 first EOF modes based on isopycnal displacements of individual surveys (c)

anomaly contain the layer where the first two most energetic EOF of isopycnal displacements do not change sign (Fig. 6b). Therefore the relative dynamic topography patterns correlate rather well with the $N_{\max}$ layer

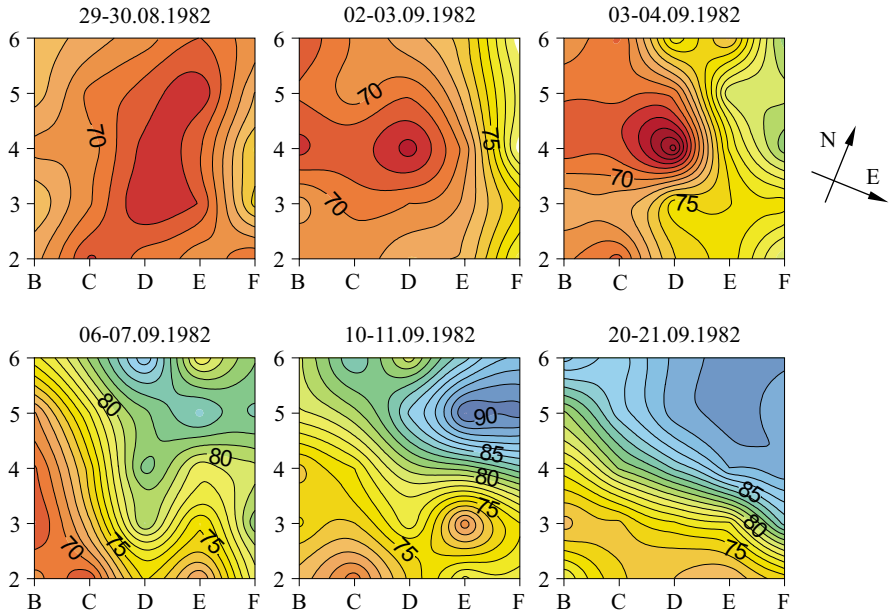

Fig. 7. Maps of the 7.0 kg m^{-3} isopycnal depth. The grid map is given in Fig. 1b (page 93)

depth patterns given in Fig. 7. Being a geostrophic stream function of relative velocity, the dynamic topography streamlines are in agreement with the low-passed observations of relative currents, as shown in Fig. 8. As the deep layers in the Baltic are not necessarily quiescent, we are careful in interpreting the dynamic topography in terms of absolute velocity. The 1st dynamic topography map reveals relative cyclonic currents that are consistent with the spreading patterns of upper layer salinity described earlier. During the 2nd and 3rd surveys a 'dynamic low' was observed at station D4. In the eastern part of the grid, an area with high dynamic topography values started to develop and widen. During the 4th, 5th and 6th surveys a well-expressed jet-like structure (of relative currents) was observed. In addition, a 'dynamic low' eddy-like structure was found at stations E5 and D5.

The 2nd mode of the mass field variability, based on the EOF structure (Fig. 6b), can be mapped by the layer thickness between the isopycnals of 7.0 kg m^{-3} (level of maximum displacement above the level of sign change) and 8.0 kg m^{-3} (the deepest well-mapped level below the level of sign change) as shown in Fig. 9. Against a background of a general south–north increase in layer thickness, an isolated lens structure can be readily distinguished by the maximum layer thickness. Based on the low-

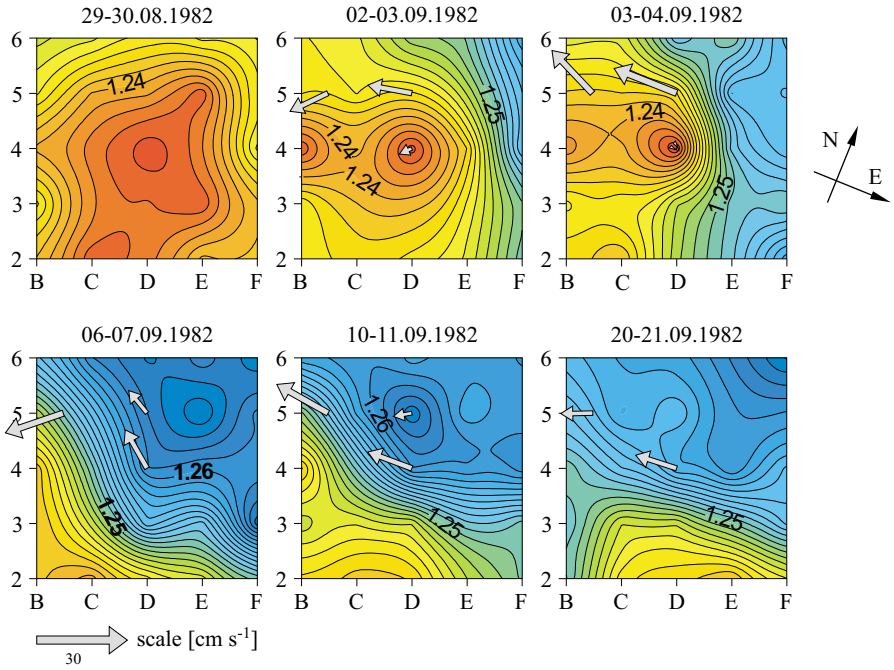

Fig. 8. Maps of dynamic topography (dynamic meter, 10 m^2 s^{-2}) of the 30 dbar level relative to the 90 dbar level and low-passed (56 h cosine filter) current vectors at 30 m depth relative to 90 m depth. The grid map is given in Fig. 1b (page 93)

pass filtered current observations at 90-m depth (shown in Fig. 9 by arrows), the lens structure was an anticyclonic second mode (subsurface) eddy that appeared during the 1st survey at station E5. During the next period it moved along the channel from east to west (stations D4 and E4, 2nd survey; stations B4 and C5, 4th survey) at an average translation speed of 2.5 nm day^{-1} (5 cm s^{-1}), to leave the study area somewhat later.

The diameter of the 2nd mode eddy was about 20 km, about twice the local Rossby deformation radius.

Cross-channel density sections during the first eddy appearance in the 2nd survey (Fig. 10) confirm that the eddy centred at stations D4–D5 had a lens-like, 2nd mode structure, with the isopycnals rising at the top of the halocline and falling in the deep layers. A similar lens-like structure was also observed at stations B4 and B5 during the 2nd survey, but compared to the lens described above, the 'undisturbed' isopycnal was 8.0 kg m^{-3} instead of 7.8 kg m^{-3}. The eddies were superimposed on tilted deeper isopycnals, with smaller depths on the southern slope of the channel. On considering the isopycnal depths in more layers during all the surveys (not shown), it becomes clear that the deepening of the halocline in the north–eastern

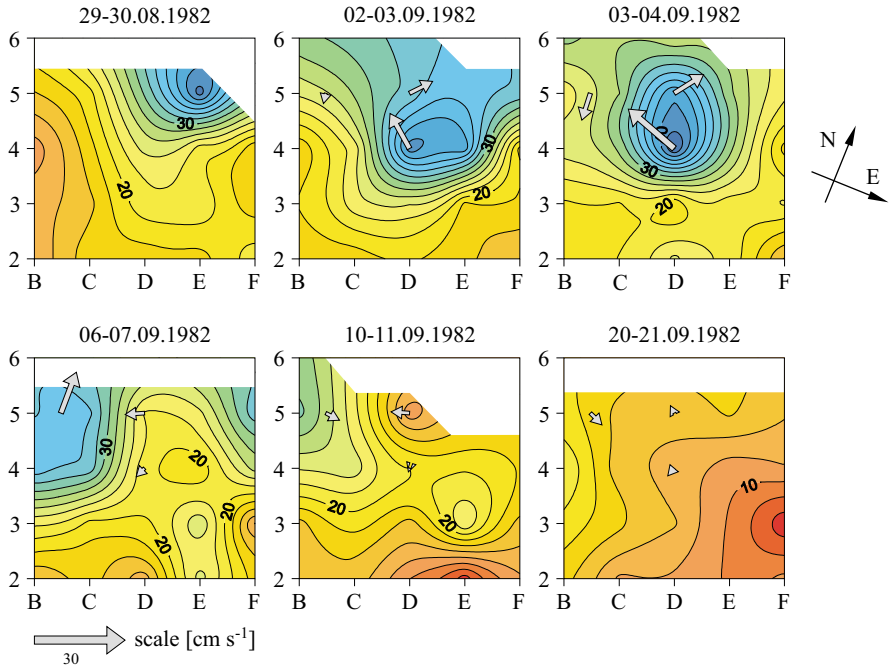

Fig. 9. Maps of layer thickness in the halocline between the isopycnals 7.0 and 8.0 kg m^{-3} and low-passed (56 h cosine filter) current vectors at 90 m depth. The grid map is given in Fig. 1b (page 93)

part of the grid started from the deep layers and then spread to the upper isopycnals of the halocline.

3.1.3. The time series of temperature and currents

The thermistor chains measured the thermocline region from 31 August to 17 September. The time series at mooring stations I and II (Fig. 11) showed that in the first days of September the thermocline was more or less stable near 20 m depth. From 4 September onwards, until 12 September, the thermocline deepened to 25–27 m depth. The thermocline began to rise at station I in the middle of September, whereas the deepening of the thermocline continued at station II. During the whole observation period, quite a lot of internal wave activity was observed at and below the thermocline. The amplitudes of these waves, mainly of near-inertial period, were typically 1–2 m.

The moored current meters showed variable currents, which were generally oriented towards the south–west. The current speed in the upper layer varied roughly between 8 and 38 cm s^{-1}, with the average speed being

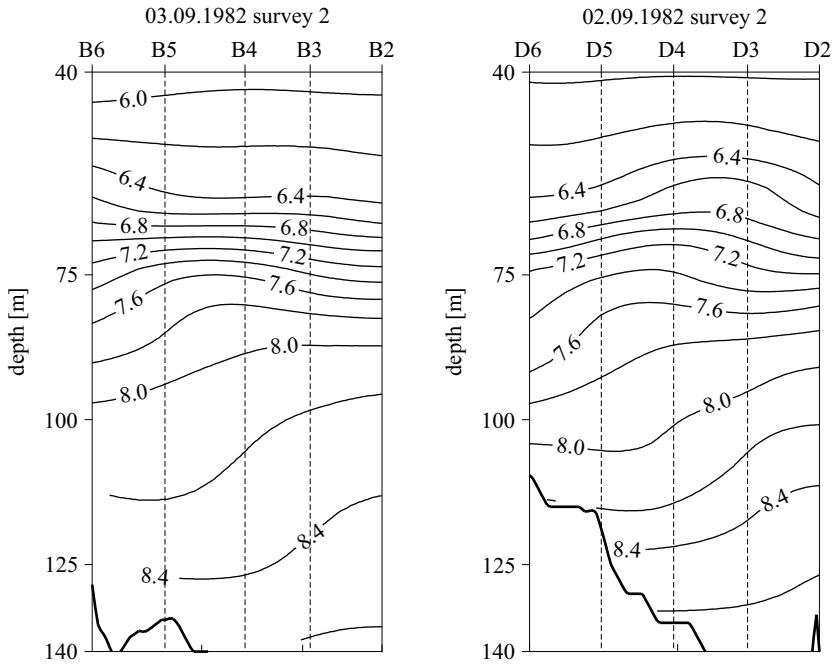

Fig. 10. Cross-channel sections of density during the 2nd survey along B (left) and D (right) (see Figs 1b and 7–9). North is on the left side of the section

21 cm s^{-1}. Just below the thermocline at 30 m depth, the current speed varied roughly between 5 and 30 cm s^{-1} around the overall mean of about 16 cm s^{-1}. In the halocline at 90 m depth, the current speed varied between the detection limit and 24 cm s^{-1}, with the average being less than 7 cm s^{-1}.

The resultant currents were flowing towards SSW, following roughly the direction of the large-scale bottom topography in the area. The stability of the current, defined as vector resultant speed divided by scalar mean speed, was 34–64% in the surface layer, 68–76% just below the thermocline and 13–52% in the halocline layer. The current was the most stable in the central area of the channel at station III. Stick-plot diagrams of the hourly mean current vectors, observed at the three mooring stations, are presented in Fig. 12.

The 90 m level lies in the halocline, where the currents are expected to be normally rather weak. However, during this experiment the halocline currents (Fig. 12) were as intensive as the currents of the thermocline. We can notice that the currents of the highest speed (about 20 cm s^{-1}) appeared first at station III on 3–4 September, and later, on 6–7 September at station I 7.5 nm to the west. The current vector rotated clockwise at stations I and II. At station III it first rotated counterclockwise and then declined rapidly

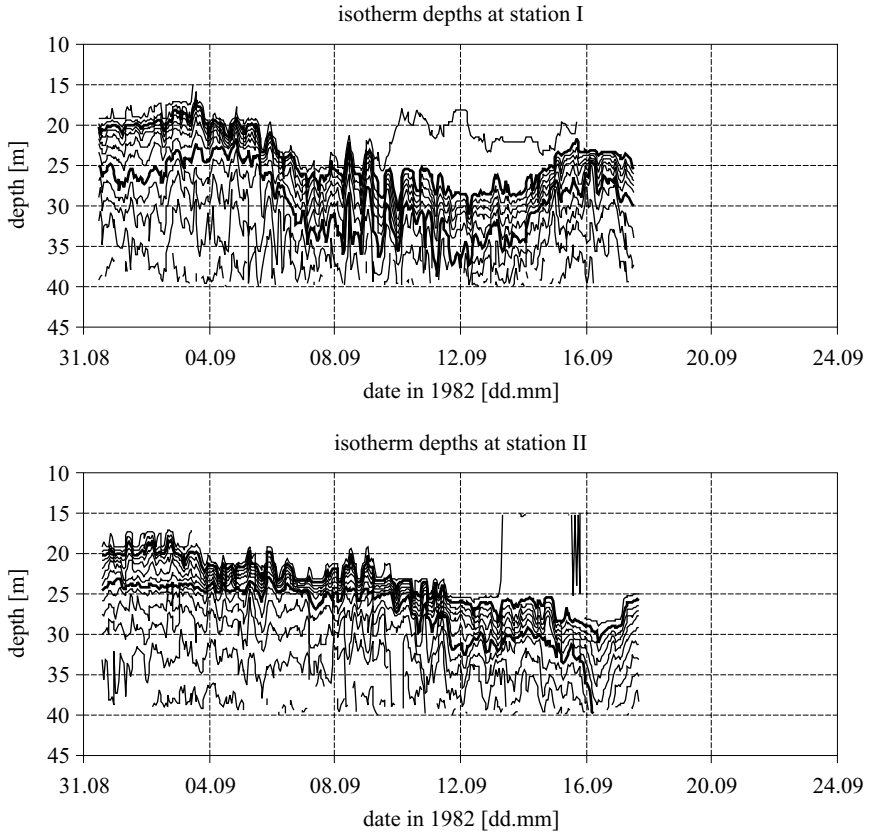

Fig. 11. Time series of isotherm depths at stations I (above) and II (below) with a 1°C interval. The 15°C and 10°C isotherms are drawn with a bold line

on 6 September. As can be seen in the maps of the region's hydrography (Fig. 7), this intense current period coincides with the deepening of the halocline (shown as the depth of $\sigma = 7.0$ kg m^{-3}) from a level of some 68 m down to 80 m. At the same time, the hydrography shows a substantial anticyclonic eddy in the region. The outburst in the current measuring sites lasted until the halocline had descended below 80 m. There were only rather weak currents after this intensive outburst. After the intense flow, moderate inertial oscillations were observed, in particular at stations II and III, lasting more than a week. This was not the case at station I, indicating an almost vanishing group velocity of the inertial waves generated near stations II and III.

The passing of a 2nd mode eddy through the array of moorings generated high values of divergence and relative vorticity. The low-passed (56-h cosine filter) divergence at 90 m depth reached $0.18f$ and the relative vorticity was

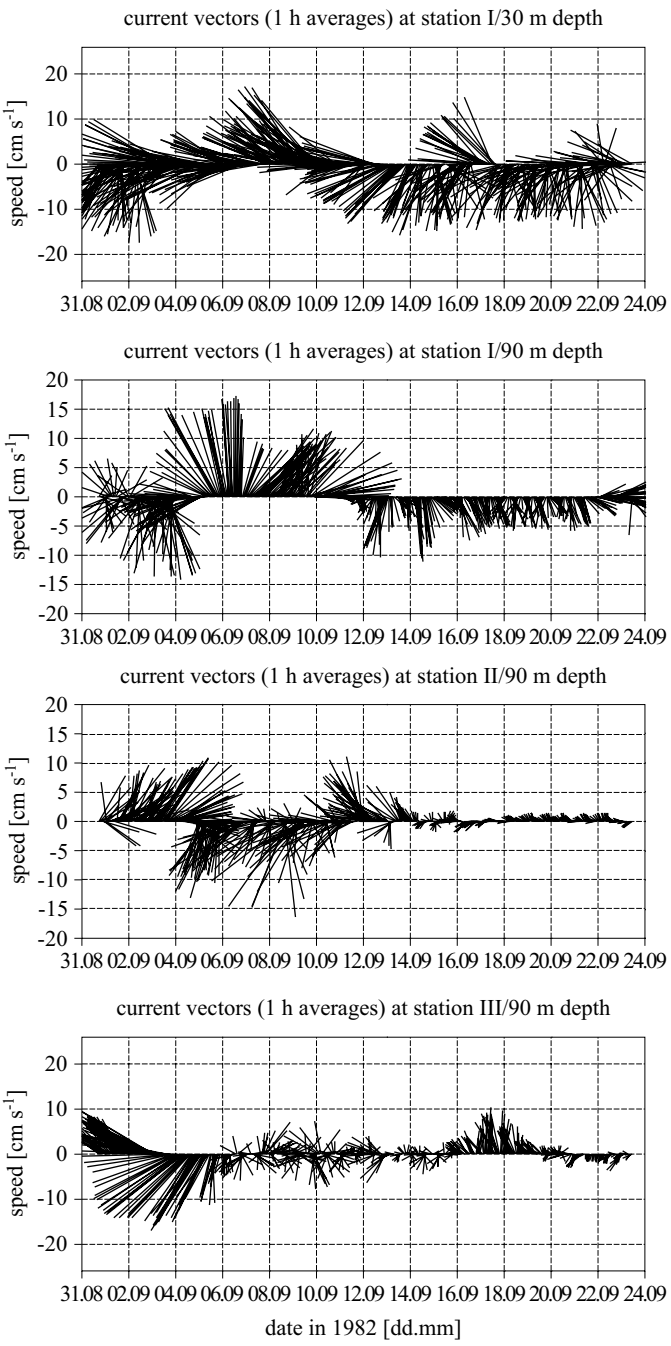

Fig. 12. Stick-plots of hourly mean current vectors. North and east are upwards and to the left, respectively

$-0.17f$, where f is the local Coriolis parameter (about 1.2×10^{-4} s^{-1}). After passing the eddy, starting from 8 September, both the divergence and the relative vorticity changed sign and performed oscillations with periods of 6–8 days and maximum absolute values around $0.1f$. Despite the high values of relative vorticity, the balance of potential vorticity was dominated by the divergence of currents and advection of relative vorticity, and the contribution of the rate of change of relative vorticity was small.

3.1.4. Interpretation of mesoscale patterns

A burst of intense deep currents at 90 m depth was observed during the rapid changes of water level in the Gulf of Finland. Before that, the gradual increase in the Gulf of Finland water storage, which occurred as a result of SW winds, temporarily changed to a rapid fall during the SE winds. The subsequent rapid increase – by 30–50 cm in a few days – resulted in a total transport rate of c. 5000 m^3 s^{-1} from the Northern Baltic Proper into the Gulf of Finland. (The average total outflow from the Gulf of Finland is 3500 m^3 s^{-1} (Alenius et al. 1998)). Because of the wind-generated origin, the depth structure of such an inflow event consists of a surface Ekman transport modified by a cross-channel sea-level difference, and a counter-estuarine transport below the Ekman layer (Elken et al. 2003).

The blocking of the standard estuarine circulation by the SW winds and significant barotropic forcing over the variable topography led to strong baroclinic signals in the halocline of the Northern Baltic Proper. The deeper isopycnals kept the tilting typical of estuarine channel flow (e.g. the Słupsk Channel, Piechura et al. 1997), in our case with higher isopycnals in the south. The counter-estuarine forcing led to the deepening of isopycnals, which started in the deep layers and then spread further through the whole halocline. The counterflow was concentrated on the northern slope of the channel, leading to an increase in the layer thickness (decrease in isopycnal potential vorticity) there. This is also similar to the Słupsk Channel, where extensive high-resolution data sets are available. In the dynamic situation, both the hydrography and the current observations reveal the onset of an anticyclonic eddy about 20 km in diameter, moving below the halocline westwards along the northern flank of the depression at an average speed of some 5 cm s^{-1}.

3.2. Stratification differences between the basins

In identifying the counter-estuarine deep flows and energetic mesoscale processes, the question is, how frequent may such events be? Over the longer 1979–98 time span, we used the time–depth gridded data from the HELCOM monitoring stations. The density difference between the Northern Baltic

Proper (BMP H2) and the entrance to the Gulf of Finland (BMP H1) revealed that negative (counter-estuarine) density differences were observed at the main halocline level quite frequently, that is, 35% of the time–depth grid values of the 40–85 m layer. Seasonally, reversals dominate during summer. Throughout the year, the median density difference ranges from 0.00 kg m^{-3} in summer to 0.19 kg m^{-3} in winter. The difference of 75% and 25% quartiles is constantly around 0.3 kg m^{-3}. Note that within the geostrophic formulation of deepwater transport between the basins, reversed density difference may also imply reversed transport.

Mesoscale variability was studied on the basis of survey and section clusters containing at least five CTD casts within no more than 5 days. The median of the r.m.s. deviation of the 7.0 kg m^{-3} isopycnal representing the mean halocline depth was calculated as 3.5 m in the Gotland Deep, 4.1 m in the Northern Baltic Proper (latitude $> 58.2°$N, longitude $< 22°$E) and 4.9 m at the entrance to the Gulf of Finland (longitude $> 22°$E). The deeper isopycnals, for example 7.5 kg m^{-3}, have the same value of mesoscale variance in the Gotland Deep, but in the Northern Deep the variance increases to 5.3 m. Towards the Gulf of Finland, deeper isopycnals were present only at mesoscale measurements conducted in summer, owing to the strong seasonal variations in the Gulf of Finland (Haapala & Alenius 1994). As a rule, a higher halocline variance occurs in the northern areas during autumn, from August to October. In the Gotland Basin, the maximum halocline variance generally occurs later, from October to December. Exceptional variances not in line with the usual seasonal behaviour occur after the major Baltic inflows.

Isopycnal temperature (as a tracer of water masses in spiceless layers, cf. Stipa 2002) did not show any regular basin-to-basin differences. The formation of deepwater masses is therefore due to the wind-induced intermittent events of lateral transport and diapycnal mixing, which occur in the basins in different ways owing to their topographic features.

3.3. Results from the operational BalEco model

The rich hydrodynamic variability in the Northern Baltic Proper during the summer and autumn of 2004 is illustrated in Figs 13 and 14 by the results from the operational BalEco numerical model with a 6 nm resolution. At the level of the halocline, salinity variations are due to the tilted isohalines, which are almost identical to the tilted isopycnals (cf. Stipa 2002).

The dominating pattern of the spatial halocline variation in the west–east direction is the upward doming (minimum halocline depth, maximum salinity) around 20.0°E throughout summer and autumn (Fig. 13a). The

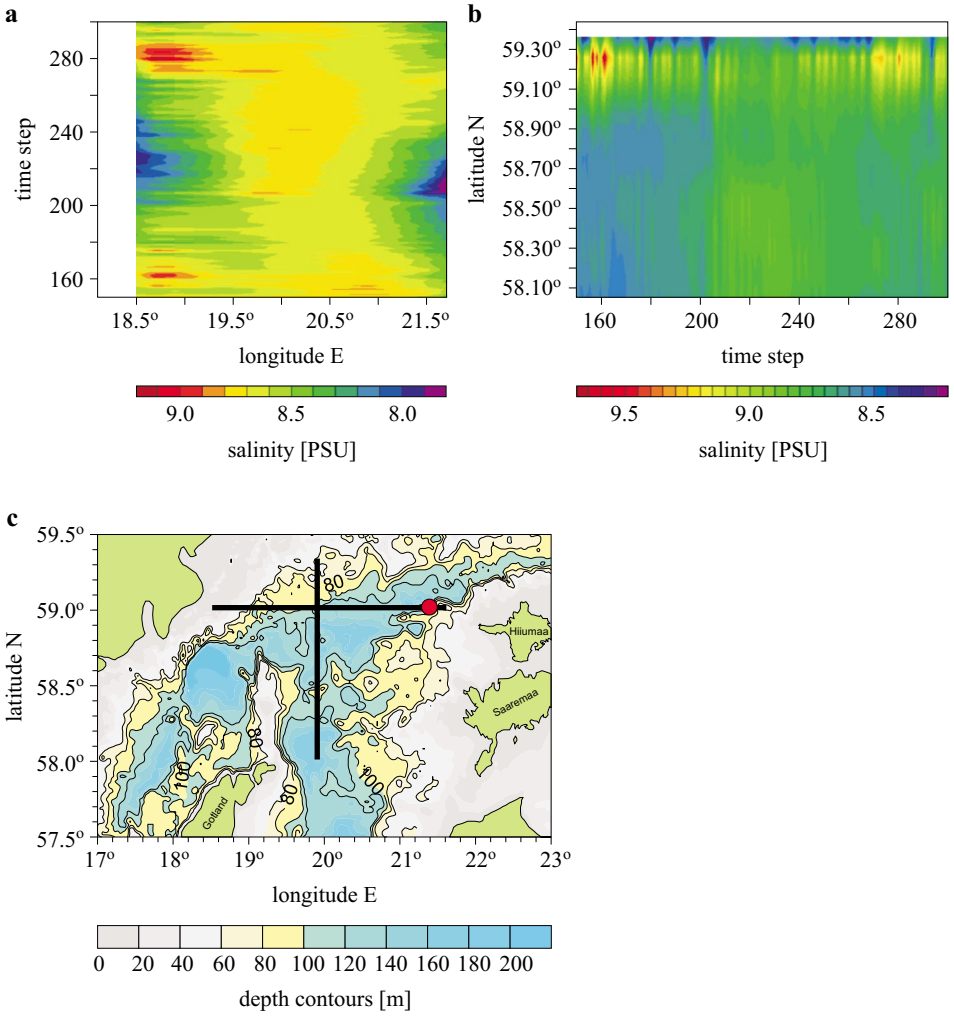

Fig. 13. Sections of salinity versus time at 67.9 m depth in the Northern Baltic: the west–east section along latitude 59.0°N (a) and the south–north section along longitude 19.9°E (b) as shown on the map (c). With two time steps per day, time step 150 is 14 June 2004

halocline is lifted up by 10 m between longitudes 19.2 and 21.2°E as compared to its depth inside the Gulf of Finland at about 21.8°E. This vertical displacement, reflecting the basin-wide circulation in the area, is associated with large changes in the isopycnal distances and corresponding changes in potential vorticity in the area. The general pattern is modified by the wind-induced structures. For example, a very deep mixed layer and halocline were modelled near the coast of the Estonian island of Hiiumaa

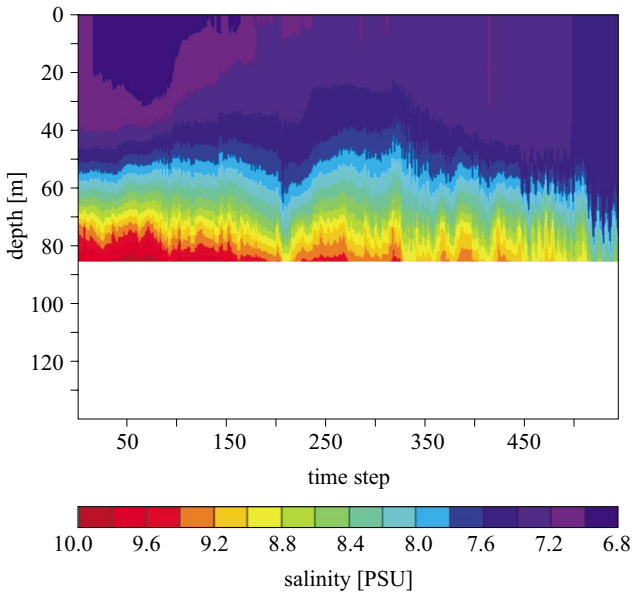

Fig. 14. Time series of salinity versus depth at 59.0°N, 21.5°E (shown in Fig. 13c by a dot) at the entrance to the Gulf of Finland. With two time steps per day, time step 0 is 1 April 2004

(59.0°N, 21.5°E) around 19 July (model time step 220). A similar structure was also observed on board r/v 'Aranda' at the same time (T. Stipa, in prep.). This feature persisted for about a month. After 20 July, in the rising phase of the deep halocline (relaxation of the downwelling) in the eastern part of the channel, the halocline started to deepen in the western part of the channel. The dome with shallow halocline depths was maintained around 20.0°E. At the end of August – beginning of September, this doming structure shifted to the west because of the deep upwelling occurring there due to SW winds.

As part of the basin-wide deep circulation, the halocline doming in the central area continues northwards by a quasi-permanent halocline deepening by about 10 m at 59.5°N. Fig. 13b depicts the variation in isobaric salinity with time and latitude. The above halocline deepening is reflected by the lower salinity values throughout the modelling period. Structures that are coherent on a smaller spatial scale are found in the model results on several occasions. Variations of about 0.5 PSU are common in the central area, but the highest variations are found on the northern boundaries. This is a manifestation of the well-known concentration of horizontal velocity divergence to the boundaries, resulting in the amplification of internal isopycnal displacements.

A time series of salinity is given in Fig. 14. The dynamic nature of this area is captured in the time series as large variations in both the halocline depth and the isopycnal spacing within the halocline itself. On the seasonal scale, the dominant signal is the strengthening/rising of the halocline during summer and its weakening/deepening during autumn, as shown also by the observational data (Haapala & Alenius 1994). This behaviour is modified by wind-induced changes as described above.

4. Discussion and conclusions

We have shown that the SW wind events, which rapidly increase water storage in the Gulf of Finland (as shown by higher water levels), generate an energetic baroclinic response in the Northern Baltic Proper. While a water storage increase means an average (over a cross-section) counter-estuarine transport in the Gulf, the deep layer is forced to flow out as a result of the continuity arguments, since the inflow takes place mainly in the Ekman surface layer. The rapidly forced barotropic flow crossing the depth contours induces isopycnal displacements, which are converted into 'new' baroclinic flow patterns due to the geostrophic adjustment, including low-frequency wave propagation and eddy generation.

In such a dynamic, temporary counter-estuarine situation, the experimental material obtained in the Northern Baltic Proper shows that the deepening of the isopycnal depths starts at the deepest levels and further on spreads to the upper isopycnals. The variability and adjustment are particularly pronounced in the deep channel entrances to the Gulf of Finland, where the inflow of saline water is enhanced by the narrow entrance with a complex topography. This is shown by the data treated in this paper, as well as by the model results, in particular by the time series at the entrance.

In the Northern Baltic Proper the mean basin-scale circulation, which is disturbed by the wind-induced events (including those that change the water storage in the neighbouring Gulf of Finland), is cyclonic (Lehmann et al. 2002, Andrejev et al. 2004). In the surface layers it is governed by the extension of the westward Finnish coastal current (Stipa 2003) and the flow of the Baltic Proper waters towards the Gulf of Finland. The latter feeds the migrating and self-restoring quasi-permanent front in the Gulf of Finland entrance area (Pavelson et al. 1997). In our study, the mean circulation is manifested by the halocline doming pattern in the Northern Deep during summer. For reference, see the 1st CTD survey in 1982 in sub-section 3.1, the basin-to-basin density differences for 1979–98 in 3.2, and the modelling results for 2004 in 3.3.

The observed mesoscale patterns, described in sub-section 3.1, are quite similar to those observed in the Słupsk Channel (Piechura et al. 1997, Zhurbas et al. 2004, Piechura et al. 2005), another deep channel of the Baltic Sea. The estuarine flow of dense water follows the right-hand slope of the channel. The counterflow takes place on the opposite slope of the channel, leading to an increase in the layer thickness (decrease in the isopycnal potential vorticity) there. The counterflow is amplified by winds of appropriate direction. The flow pulses generate strong sub-surface eddies in both channels.

As far as the advective–diffusive balance of the water cycle in the Northern Baltic is concerned, we argue that meso- and basin-scale lateral transport processes are of great importance for diapycnal mixing in the halocline. Historically, many researchers have said that during stagnation periods, stratification in the Northern Baltic becomes so weak that ventilation of deep layers by oxygen-rich waters takes place by 'vertical' convective and/or wind-induced mixing of the water column. Although effective diapycnal mixing in the area has not been not quantitatively considered to the full, our study suggests that it is hardly possible without lateral, vorticity-affected processes being involved. The pulses of SW winds generate a sequence of processes:

- the increase in water storage in the Gulf of Finland generates an outflow of deep water from the Gulf;
- counter-estuarine transports in the surface and deep layers reduce the vertical stability of the water column in the Gulf of Finland but also in the Northern Deep, allowing more efficient diapycnal mixing with the same energy input;
- over a variable topography, basin-scale barotropic flows are converted into baroclinic mesoscale motions of large isopycnal displacement (>20 m within a distance of 10–20 km) and high intra-halocline current speeds (>20 cm s^{-1}).

So far, we have not performed high-resolution measurements down to the sea bottom. Using an example from Stigebrandt et al. (2002), we may assume that large up- and downward motions of isopycnals, intersecting the sloping 'rough' bottom, give rise to a higher intensity of diapycnal mixing in the Northern Baltic Proper as well.

The multitude of processes at the entrance to the Gulf of Finland certainly causes problems in the modelling of the deep water inflow, e.g. by enhancing internal wave activity, the production of strong eddies and topographic waves and, through these processes, increasing diapycnal mixing. These processes are not always resolved in a proper way, as many

numerical models in which mixing is 'tuned' to observations in the Gotland Deep produce too strong a stratification in the Gulf of Finland as compared to the observations.

In comparison to other basins of the Baltic Sea, the bottom layers of the entrance region of the Gulf of Finland seem to be rather active in response to wind forcing. This does not agree with the earlier ideas of partially decoupled lower layer dynamics.

References

Aitsam A., Elken J., 1982, *Synoptic scale variability of hydrophysical fields in the Baltic Proper on the basis of CTD measurements*, [in:] *Hydrodynamics of semi-enclosed seas*, J. C. J. Nihoul (ed.), Elsevier, Amsterdam, 433–468.

Aitsam A., Hansen H. P., Elken J., Kahru M., Laanemets J., Pajuste M., Pavelson J., Talpsepp L., 1984, *Physical and chemical variability of the Baltic Sea: a joint experiment in the Gotland Basin*, Cont. Shelf Res., 3 (3), 291–310.

Alenius P., Myrberg K., Nekrasov A., 1998, *The physical oceanography of the Gulf of Finland: a review*, Boreal Environ. Res., 3 (2), 97–125.

Alenius P., Nekrasov A., Myrberg K., 2003, *Variability of the baroclinic Rossby radius in the Gulf of Finland*, Cont. Shelf Res., 23 (6), 563–573.

Andrejev O., Myrberg K., Alenius P., Lundberg P. A., 2004, *Mean circulation and water exchange in the Gulf of Finland – a study based on three-dimensional modeling*, Boreal Environ. Res., 9 (1), 1–16.

Dietrich G., 1948, *Der jährliche Gang der Temperatur- und Salzgehaltsschichtung in den britischen Randmeeren und in der Nord- und Ostsee*, Wiss. Ber. Dt. Hydrogr. Inst., Hamburg, 80 pp.

Elken J. (ed.), 1996, *Deep water overflow, circulation and vertical exchange in the Baltic Proper*, Est. Mar. Inst. Rep. Ser. No 6 (Tallinn), 1–91.

Elken J., Raudsepp U., Lips U., 2003, *On the estuarine transport reversal in deep layers of the Gulf of Finland*, J. Sea Res., 49 (4), 267–274.

Fennel W., Seifert T., Kayser B., 1991, *Rossby radii and phase speeds in the Baltic Sea*, Cont. Shelf Res., 11 (1), 23–36.

Gustafsson B. G., Andersson H. C., 2001, *Modelling the exchange of the Baltic Sea from the meridional atmospheric pressure difference across the North Sea*, J. Geophys. Res., 106 (C9), 19731–19744, doi: 10.1029/2000JC000593.

Haapala J., Alenius P., 1994, *Temperature and salinity statistics for the Northern Baltic Sea 1961–1990*, Finn. Mar. Res., 262, 51–121.

HELCOM, 2002, *Environment of the Baltic Sea area, 1994–1998*, Baltic Mar. Environ. Prot. Commiss., Helsinki, 82B, 215 pp.

Huang R. X., 1998, *Mixing and available potential energy in a Boussinesq ocean*, J. Phys. Oceanogr., 28 (4), 669–678.

ICES, 1989, *The Baltic Sea Patchiness Experiment – PEX '86*, ICES Coop. Res. Rep. No 163, Vols 1–2 , 100 + 156 pp.

Kiiltomäki A., Stipa T., 2006, *High resolution validation for an operational hydrodynamical model in the Baltic Sea*, Cont. Shelf Res., (submitted).

Kiiltomäki A., Stipa T., Kaitala S., 2005, *Temporal and spatial variation of dissolved nutrients in the Baltic Sea in 2004*, HELCOM Indicator Fact Sheets, http://www.helcom.fi/environment2/ifs/ifs2005/en_GB/dissolved_nutrients/.

Kõuts T., Omstedt A., 1993, *Deep water exchange in the Baltic Proper*, Tellus A, 45 (4) 311–324.

Lass H. U., Prandke H., Liljebladh B., 2003, *Dissipation in the Baltic Proper during winter stratification*, J. Geophys. Res., 108 (C6), 3187, doi: 10.1029/2002JC001401.

Lehmann A., Hinrichsen H.-H., 2002, *Water, heat and salt exchange between the deep basins of the Baltic Sea*, Boreal Environ. Res., 7 (4), 405–415.

Lehmann A., Krauss W., Hinrichsen H.-H., 2002, *Effects of remote and local atmospheric forcing on circulation and upwelling in the Baltic Sea*, Tellus A, 54 (3), 299–316.

Marshall J., Adcroft A., Hill C., Perelman L., Heisey C., 1997, *A finite-volume, incompressible Navier Stokes model for studies of the ocean on parallel computers*, J. Geophys. Res., 102 (C3), 5753–5766, doi: 10.1029/96JC02775.

Matthäus W., 1984, *Climatic and seasonal variability of oceanological parameters in the Baltic Sea*, Beitr. Meereskund., 51, 29–49.

Matthäus W., Franck H., 1992, *Characteristics of major Baltic inflows – a statistical analysis*, Cont. Shelf Res., 12 (12), 1375–1400.

Meier H. E. M., Kauker F., 2003, *Modeling decadal variability of the Baltic Sea: 2. Role of freshwater inflow and large-scale atmospheric circulation for salinity*, J. Geophys. Res., 108 (C11), 3368, doi: 10.1029/2003JC001799.

Omstedt A., Elken J., Lehmann A., Piechura J., 2004, *Knowledge of the Baltic Sea physics gained during the BALTEX and related programmes*, Prog. Oceanogr., 63 (1–2), 1–28.

Pavelson J., Laanemets J., Kononen K., Nõmmann S., 1997, *Quasi-permanent density front at the entrance to the Gulf of Finland: response to wind forcing*, Cont. Shelf Res., 17 (3), 253–265.

Piechura J., Beszczyńska-Möller A., 2004, *Inflow waters in the deep regions of the southern Baltic Sea – transport and transformations*, Oceanologia, 46 (1), 113–141.

Piechura J., Walczowski W., Beszczyńska-Möller A., 1997, *On the structure and dynamics of the water in the Słupsk Furrow*, Oceanologia, 39 (1), 35–54.

Saucier F. J., Dionne J., 1998, *A 3D coupled ice-ocean model applied to Hudson Bay, Canada: the seasonal cycle and time-dependent climate response to atmospheric forcing and runoff*, J. Geophys. Res., 103 (C12), 27689–27705, doi: 10.1029/98JC02066.

Stigebrandt A., Gustafsson B. G., 2003, *Response of Baltic Sea to climate change – theory and observations*, J. Sea Res., 49 (4), 243–256.

Stigebrandt A., Lass H.-U., Liljebladh B., Alenius P., Piechura J., Hietala R., Beszczyńska A., 2002, *DIAMIX – an experimental study of diapycnal deepwater mixing in the virtually tideless Baltic Sea*, Boreal Environ. Res., 7 (4), 363–369.

Stipa T., 2002, *Temperature as a passive isopycnal tracer in salty, spiceless oceans*, Geophys. Res. Lett., 29 (20), 1953, doi: 10.1029/2001GL014532.

Stipa T., 2004, *Baroclinic adjustment in the Finnish coastal current*, Tellus A, 56 (1), 79–87.

Stipa T., Skogen M., Hansen I. S., Eriksen A., Hense I., Kiiltomäki A., Søiland H., Westerlund A., 2003, *Short-term effects of nutrient reductions in the North Sea and Baltic Sea as seen by an ensemble of numerical models*, Finn. Inst. Mar. Res. Rep. Ser. No 49, 43–70.

Tian R., Vézina A. F., Starr M., Saucier F. J., 2001, *Seasonal dynamics of coastal ecosystems and export production at high latitudes: a modeling study*, Limnol. Oceanogr., 46 (8), 1845–1859.

Winsor P., Rodhe J., Omstedt A., 2001, *Baltic Sea ocean climate: an analysis of 100 yr of hydrographic data with focus on the freshwater budget*, Climate Res., 18 (1–2), 5–15.

Zhurbas V., Stipa T., Mälkki P., Paka V., Golenko N., Hense I., Sklyarov V., 2004, *Generation of subsurface cyclonic eddies in the southeast Baltic Sea: observations and numerical experiments*, J. Geophys. Res., 109 (C05033), doi: 10.1029/2003JC002074.